Structural determinants in phycotoxins and AChBP conferring high affinity binding and nicotinic AChR antagonism

Yves Bourne[a,1], Zoran Radić[b], Rómulo Aráoz[c], Todd T. Talley[b], Evelyne Benoit[c], Denis Servent[d], Palmer Taylor[b], Jordi Molgó[c], and Pascale Marchot[e,1]

[a]Architecture et Fonction des Macromolécules Biologiques, Centre National de la Recherche Scientifique, Université d'Aix-Marseille, Campus Luminy–Case 932, F-13288 Marseille Cedex 9, France; [b]Department of Pharmacology, Skaggs School of Pharmacy and Pharmaceutical Sciences, University of California at San Diego, La Jolla, CA 92093-0657; [c]Laboratoire de Neurobiologie Cellulaire et Moléculaire, Centre National de la Recherche Scientifique, Institut de Neurobiologie Alfred Fessard–FRC2118, F-91198 Gif-sur-Yvette Cedex, France; [d]Institut de Biologie et Technologies de Saclay, Service d'Ingénierie Moléculaire des Protéines, Laboratoire de Toxinologie Moléculaire, Commissariat à l'Energie Atomique, F-91191 Gif-sur-Yvette, France; and [e]Centre de Recherche en Neurobiologie-Neurophysiologie de Marseille, Centre National de la Recherche Scientifique, Université d'Aix-Marseille, Institut Fédératif de Recherche Jean Roche, Faculté de Médecine–Secteur Nord, CS80011, F-13344 Marseille Cedex 15, France

Edited* by William A. Catterall, University of Washington School of Medicine, Seattle, WA, and approved February 17, 2010 (received for review October 26, 2009)

Spirolide and gymnodimine macrocyclic imine phycotoxins belong to an emerging class of chemical agents associated with marine algal blooms and shellfish toxicity. Analysis of 13-desmethyl spirolide C and gymnodimine A by binding and voltage-clamp recordings on muscle-type $\alpha1_2\beta\gamma\delta$ and neuronal $\alpha3\beta2$ and $\alpha4\beta2$ nicotinic acetylcholine receptors reveals subnanomolar affinities, potent antagonism, and limited subtype selectivity. Their binding to acetylcholine-binding proteins (AChBP), as soluble receptor surrogates, exhibits picomolar affinities governed by diffusion-limited association and slow dissociation, accounting for apparent irreversibility. Crystal structures of the phycotoxins bound to *Aplysia*-AChBP (≈2.4Å) show toxins neatly imbedded within the nest of aromatic side chains contributed by loops C and F on opposing faces of the subunit interface, and which in physiological conditions accommodates acetylcholine. The structures also point to three major features: (*i*) the sequence-conserved loop C envelops the bound toxins to maximize surface complementarity; (*ii*) hydrogen bonding of the protonated imine nitrogen in the toxins with the carbonyl oxygen of loop C Trp147 tethers the toxin core centered within the pocket; and (*iii*) the spirolide *bis*-spiroacetal or gymnodimine tetrahydrofuran and their common cyclohexene-butyrolactone further anchor the toxins in apical and membrane directions, along the subunit interface. In contrast, the sequence-variable loop F only sparingly contributes contact points to preserve the broad receptor subtype recognition unique to phycotoxins compared with other nicotinic antagonists. These data offer unique means for detecting spiroimine toxins in shellfish and identify distinctive ligands, functional determinants and binding regions for the design of new drugs able to target several receptor subtypes with high affinity.

acetylcholine binding protein | marine phycotoxins | nicotinic acetylcholine receptor | pharmacological and structural analyses | seafood poisoning

Marine algal toxins and the associated phytoplankton species are responsible for >60,000 toxicity incidents worldwide per year with a mortality rate of 1.5%. The major source of these bioactive toxins is unicellular algae that proliferate to form dense cell concentrations or "blooms." When deposited throughout the marine environs by emptying of ship ballasts, harmful algal blooms are associated with the demise of wildlife, including birds and marine mammals. The toxins also move up the food chain through shellfish, a rich worldwide food resource: Shellfish contaminated by toxins serve to concentrate and direct them to animals and humans (1). Given their capacity to cross the blood–brain barrier (2), their lipophilic properties and their modest volatility, when concentrated they represent an environmental and human health risk and a threat to the fishery industry. However, the complexity of their chemical synthesis (3) has hampered studies on their mechanism(s) of action.

Spirolides (Fig. 1) are a family of unique macrocyclic imine phycotoxins detected in North American and European coasts, first isolated from the digestive glands of mussels, scallops, and phytoplankton harvested from aquaculture sites (4–6). The dinoflagellate *Alexandrium ostenfeldii* has been associated to spirolide production (4, 7–9). Spirolides contain an unusual 5,5,6-*bis*-spirocetal moiety embedded within a 23-membered macrocycle along with a 6,7-spirocyclic imine structure that is found in related gymnodimines, pinnatoxins, and pteriatoxins (10). They exhibit rapid lethality associated with central neurological symptoms when administered i.p. or p.o. to mice (2, 11).

Gymnodimines (Fig. 1) have been identified from contaminated shellfish or from extracts of the dinoflagellate *Karenia selliformis* (12–15). Similar to spirolides, gymnodimines contain a spirocyclic imine but, in contrast to spirolides, they bear a trisubstituted tetrahydrofuran embedded within a 16-membered macrocycle. Gymnodimines also cause rapid neurotoxic mortality (15, 16).

Initial research into the mode of action of spirolides A-D had suggested that they are antagonists of muscarinic acetylcholine (ACh) receptors (11). Later reports revealed that 13-desmethyl spirolide C caused dose-dependent, widespread mouse brain neuronal damage and up-regulation of muscarinic and nicotinic ACh receptors (nAChR) transcription in rats (2). In contrast to most peptidic toxins, gymnodimines target both muscle and neuronal nAChRs at subnanomolar concentrations, explaining their neurotoxicity (15).

The nAChRs are prototypical cation-selective, ligand-gated ion channels (LGIC) that mediate fast neurotransmission in the central and peripheral nervous systems (17, 18). They belong to the Cys-loop superfamily of LGICs and are formed by distinct combinations of five subunits that confer selectivity in pharmacological properties and cellular location (19).

The soluble ACh-binding proteins (AChBP) from mollusks form homopentameric assemblies of subunits homologous to the N-terminal, extracellular ligand-binding domain (LBD) of the nAChR (20–22) (Fig. S1). In addition to the overall structural features of the subunits, the aromatic side chains that form the ligand binding pocket at the subunit interfaces are well conserved in the nAChR family, with greater variability for residues at the complementary or (-) face than

Author contributions: Y.B., P.T., J.M., and P.M. designed research; Y.B., Z.R., R.A., T.T.T., E.B., D.S., J.M., and P.M. performed research; Y.B., Z.R., D.S., P.T., J.M., and P.M. analyzed data; and Y.B., D.S., P.T., J.M., and P.M. wrote the paper.

The authors declare no conflict of interest.

*This Direct Submission article had a prearranged editor.

Data deposition: The atomic coordinates and structure factors of the SPX and GYM complexes with *Aplysia californica* AChBP have been deposited in the Protein Data Bank, www.pdb.org (PDB codes 2WZY and 2X00, respectively).

[1]To whom correspondence may be addressed. E-mail: yves.bourne@afmb.univ-mrs.fr or pascale.marchot@univmed.fr.

This article contains supporting information online at www.pnas.org/cgi/content/full/0912372107/DCSupplemental.

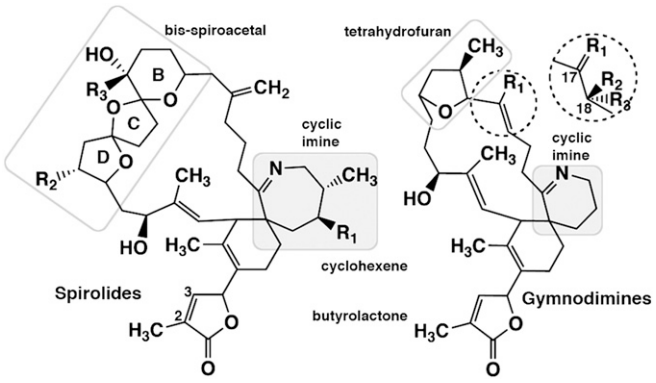

Fig. 1. Chemical structures of the spirolides (*Left*) and gymnodimines (*Right*). The seven- and six-membered cyclic imines common to the phycotoxins are highlighted with a gray background, and the chemical groups specific to each are boxed. Locations of group substitutions that differ among the various spirolides and gymnodimines are indicated. SPX (13-desmethyl spirolide C): R_1 = CH_3, R_2 = H, R_3 = CH_3. GYM (gymnodimine A): R_1 = CH_3. Substitutions found in SPX and GYM congeners are described in the *SI Appendix*.

the principal or (+) face of each interface. The binding pocket of AChBP possesses all of the functional residues identified in the nAChR LBD, and its extension toward apical and "membrane" directions of the interface provides multiple means for selective accommodation of nicotinic full and partial agonists and competitive antagonists (21, 23–25). Overall, agonists recognize a "core agonist signature motif" central to the binding pocket, whereas the larger antagonists extend toward the apical or the membrane directions along the interface, resulting in opening of loop C on the (+) face and often in greater subtype selectivity than seen for agonists.

To delineate the molecular determinants that govern the selectivity of the phycotoxins for the various homologous and orthologous nAChR species and their neurotoxicity, we performed comprehensive pharmacological and structural studies of two representative members, 13-desmethyl spirolide C (SPX) from *A. ostenfeldii*, and gymnodimine A (GYM) from *K. selliformis* (Fig. 1). Their binding affinities and potencies as antagonists toward membrane-embedded muscle-type $\alpha1_2\beta\gamma\delta$ and neuronal α3β2 and α4β2 nAChRs were examined through competition binding assays and voltage-clamp recordings. Complementary kinetic and equilibrium binding assays on AChBPs from *Aplysia californica* (A-AChBP) and *Lymnaea stagnalis* (L-AChBP) were performed by using stopped-flow instrumentation and conventional competition binding. Moreover, crystal structures of A-AChBP complexes with SPX and GYM were solved at 2.5/2.4 Å resolution. The structures, and their comparison with earlier structures of AChBP bound to agonists and antagonists, illustrate how the binding pocket is perfectly shaped to accommodate appropriately positioned macrocyclic imine toxins while preserving broad receptor subtype recognition.

Hence, although the linkage from the snail AChBPs to the mammalian nAChRs shows relevance to human pharmacology and toxicology, our studies identify distinctive ligands, functional determinants, and binding regions conferring nAChR subtype selectivity and demonstrate how the chemical features of these nicotinic antagonists present an environmental risk.

Results and Discussion

The nAChR from *Torpedo* electric organ, a prototype of vertebrate skeletal muscle receptors, is a transmembrane heteropentameric protein composed of four homologous subunits with a $\alpha1_2\beta\gamma\delta$ stoichiometry. Two binding sites with distinctive affinities for most of the nicotinic agonists and competitive antagonists are located at the α-γ and α-δ subunit interfaces. The human α3β2 and α4β2 subtypes, which play a predominant role in both pre- and postsynaptic functions in the central and peripheral nervous systems, may have variable stoichiometries involving at least two ligand binding sites at the α-β subunit interfaces. Typically, agonist binding to the two sites in the closed state induces a sequence of conformational transitions leading to channel opening followed by nAChR desensitization. Competitive antagonist binding to a single site is sufficient to block channel function. When the two sites have different affinities, competitive antagonism of function correlates with occupation of the higher affinity site (26).

Characteristics of SPX and GYM Binding to nAChRs. Binding of the phycotoxins SPX and GYM to the muscle-type $\alpha1_2\beta\gamma\delta$ and neuronal α3β2 and α4β2 nAChRs expressed in mammalian cells was recorded by competition against labeled peptidic antagonist, α-bungarotoxin, and alkaloid agonist, epibatidine. Subnanomolar dissociation constants were obtained (Table 1). In fact, the α3β2 subtype displays one order of magnitude higher affinity for SPX compared with GYM, whereas the other two nAChR subtypes do not discriminate significantly between the two toxins. This feature suggests common toxin interactions among these subtypes.

Functional analysis of SPX and GYM used voltage-clamp recordings on *Xenopus* oocytes either transplanted with $\alpha1_2\beta\gamma\delta$-enriched membranes or transfected with α4β2-encoding cDNAs (Fig. 2). The EC_{50} values determined for ACh responses attest to functionality of both nAChR, as discussed in the *SI Appendix*. SPX alone (0.5–50 nM) has no effect on oocytes with incorporated $\alpha1_2\beta\gamma\delta$ or expressing α4β2, indicating an absence of agonist activity, but it induces a dose-dependent decrease in the peak amplitudes of the ACh-elicited current on these nAChR subtypes (Fig. 2 *A* and *B* and Table 2). This antagonist activity by SPX is not abolished after a 30- to 40-min washout. Similarly, GYM shows a concentration dependent inhibition of ACh-induced currents in the $\alpha1_2\beta\gamma\delta$ oocytes (Fig. 2 *C* and *D* and Table 2). Antagonism by GYM is consistent with data obtained on *Xenopus* myocytes and frog and mouse neuromuscular preparations (15). GYM also antagonizes ACh in oocytes expressing α4β2. In contrast to SPX, GYM antagonism is readily abolished by washout. The Hill coefficients and their relationship to binding site occupancy, as well as data from a control assay with the reference antagonist, D-tubocurarine, are discussed in the *SI Appendix*.

Dissociation constants (K_i) were determined in competition binding assays (Table 1) performed at equilibrium while constants for functional antagonism (IC_{50}) determined electrophysiologically (Table 2) more closely reflect the initial association of phycotoxin interaction with the nAChR. Hence, differences in the two parameters may arise from achieving equilibrium versus nonequilibrium conditions (especially where the on rate is slow) in addition to differing incubation conditions. Yet the values, which differ ≈6.5-fold for SPX and from 1.5 to 12-fold for GYM, are within a usual 10-fold range for values obtained by binding and voltage-clamp assays. Furthermore, SPX and GYM display only slightly higher binding affinity and functional potency, by ≈7.5-fold and ≈2.9-fold, respectively, toward $\alpha1_2\beta\gamma\delta$ compared with α4β2, while SPX displays fourfold and by ≈30-fold higher affinities for α3β2 compared with $\alpha1_2\beta\gamma\delta$ and α4β2. Hence, the SPX and GYM toxins display high affinities and potent antagonism,

Table 1. Competition binding constants for SPX and GYM with muscle-type and neuronal nAChRs expressed in HEK293 cells

Ligand	K_i ± SEM, nM*		
	$\alpha1_2\beta\gamma\delta$ (Torpedo)	α4β2 (Human)	α3β2 (Human)
SPX	0.080 ± 0.002	0.58 ± 0.07	0.021 ± 0.005
GYM	0.23 ± 0.08	0.62 ± 0.07†	0.24 ± 0.09†

*Mean values ± SEM from three distinct experiments performed in duplicate.
†Calculated from IC_{50} values reported in ref. 15.

PHARMACOLOGY

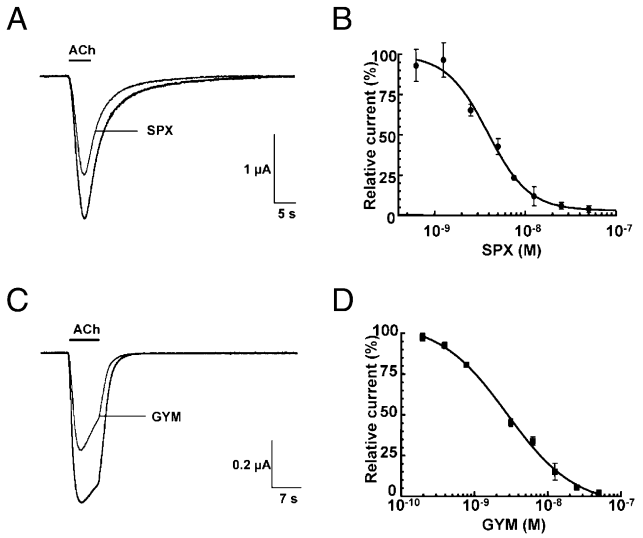

Fig. 2. Inhibition of ACh-evoked currents from neuronal and muscle-type nAChRs by the phycotoxins. SPX with human α4β2 expressed in oocytes (*A* and *B*); GYM with *Torpedo* $\alpha1_2\beta\gamma\delta$ incorporated into the oocyte membrane (*C* and *D*). (*A* and *C*) Typical inward nicotinic currents evoked by a 5-s perfusion of 150 μM ACh (EC_{50} value for α4β2) before and after application of 1.5 nM SPX (*A*), and a 7-s perfusion of 25 μM ACh (EC_{50} value for $\alpha1_2\beta\gamma\delta$) before and after application of 1.5 nM GYM (*C*). The desensitization component typical of $\alpha1_2\beta\gamma\delta$ is not modified in presence of the toxin. (*B* and *D*) SPX (*B*) and GYM (*D*) concentration-to-current inhibition relationships. The amplitudes of the ACh-induced currents recorded in the presence of SPX and GYM (mean ± SEM; 3–4 oocytes per concentration) were normalized to control currents and fitted to the Hill equation. SPX on α4β2: IC_{50} = 3.87 ± 1.1 nM; nH = 1.9 ± 0.33; GYM on $\alpha1_2\beta\gamma\delta$: IC_{50} = 2.8 ± 1.15 nM; nH = 0.96 ± 0.15 (compare Table 2).

but limited selectivity for the muscle-type versus neuronal subtypes of receptors.

Kinetic and Equilibrium Binding of SPX and GYM to AChBP. Association of SPX and GYM to A- and L-AChBPs is accompanied by quenching of the intrinsic Trp fluorescence of AChBP, consistent with the bound toxin affecting the connectivity of the aromatic side chains in the binding pocket (22). Quenching was sufficient to measure complex formation by stopped-flow kinetic and, in some cases, equilibrium titration methods. A scintillation proximity assay was used to ascertain the kinetic constants for the slow dissociating complexes and confirm the equilibrium constants for the lower affinity complexes (Table 3).

Binding data reveal high affinities of the two phycotoxins for the two AChBPs with differences being primarily reflected in the dissociation rate constants, k_{off}, which for L-AChBP range over two orders of magnitude (Table 3). For the GYM–L-AChBP complex, the low k_{off} yields a half-time for dissociation extending to 3 h. All of the bimolecular association rate constants, k_{on}, approach the diffusion limitation with the probable exception of SPX association with L-AChBP, being one order of magnitude slower. These association rate constants differ from those observed for the other high affinity and selective ligands for the nAChRs and AChBPs, such as the peptidic α-conotoxins and α-neurotoxins, where rates are 2–3 orders of magnitude below the diffusion limitation (27). Such differences might be best explained in terms of the peptide toxins selecting unique, minor abundance conformations upon binding.

Toxin selectivity is also seen among the two AChBPs studied, where the ratio of affinities for SPX versus GYM is ≈1,000-fold greater for L-AChBP, a difference that mainly reflects the 200-fold higher dissociation rate (Table 3 and Table S1). In contrast, the GYM toxin has a similar high affinity (picomolar K_d values) for the two AChBPs. In L-AChBP, the bulkier Tyr164 side chain corresponding to A-AChBP Ser167 in loop F (Fig. S1) is positioned to contribute to the higher affinity for GYM compared with SPX without causing steric clashes. Similarly, Trp53 in loop D of L-AChBP and corresponding to Tyr55 in A-AChBP may contribute to the affinity difference between L- and A-AChBPs, as found for other ligands (24, 27). In fact, the AChBPs have higher affinities for GYM than the full-length nAChR subtypes assayed herein. Whether this feature reflects specific targeting of invertebrate species by the *K. selliformis* dinoflagellate is unknown.

Overall View of the Structures. Structures of A-AChBP complexes with SPX and GYM (Fig. 3) were solved at 2.5–2.4 Å resolution (Table S2). The two structures show the tight homopentameric ring assembly of subunits found in all AChBP structures (20, 21, 23–25). The ligand binding pocket encompasses a nest of five electron-rich aromatic side chains provided by residues Tyr93, Trp147, Tyr188, Tyr195 on the (+) face and residue Tyr55 on the (-) face of the interface (Fig. S1). This pocket is partially sheltered from the solvent by loop C, which is found at the outer perimeter of the pentamer and harbors at its tip a disulfide bridge linking the vicinal Cys190 and Cys191 residues, a signature determinant for nAChR α subunits.

The two structures show very similar ligand orientations at the five subunit interfaces within a pentamer (compare rmsd values in *Materials and Methods*). The well-defined electron densities reveal full phycotoxin occupancy at all five binding sites (Fig. 3), consistent with their high affinities (Table 3).

The Spirolide–AChBP Complex. SPX, with its subnanomolar K_i and nanomolar IC_{50} values for muscle $\alpha1_2\beta\gamma\delta$ and neuronal α3β2 and α4β2 nAChRs (Tables 1 and 2), is the most potent general non-peptidic nicotinic antagonist. At the AChBP interface, the SPX bulky spirolide skeleton, with its conical shape of overall dimensions 15 × 6 × 6 Å, is oriented with its long axis roughly aligned parallel with the pentamer 5-fold axis (Fig. 3). The *bis*-spiroacetal ring system points in an apical direction along the interface, whereas the butyrolactone moiety, at the opposite end of the molecule, is oriented in the membrane direction. The *bis*-spiroacetal framework bends toward the central cyclic imine ring and comfortably accommodates the shape of the binding pocket. This orientation and conformation of the SPX

Table 2. Inhibition constants for SPX and GYM on ACh-evoked nicotinic currents in oocytes transplanted with muscle-type $\alpha1_2\beta\gamma\delta$ nAChR or expressing the neuronal α4β2 subtype

Ligand	IC_{50}, nM*	
	$\alpha1_2\beta\gamma\delta$ (Torpedo)	α4β2 (Human)
SPX	0.51 (0.4–0.6)	3.9 (2.9–5.1)
GYM	2.8 (1.9–4.1)	0.9 (0.6–1.2)

For further details *cf* Fig. 2.
*Mean values (95% confidence intervals) from concentration-response curves recorded on 24–36 oocytes for each condition.

Table 3. Kinetic constants for association (k_{on}) and dissociation (k_{off}) and calculated equilibrium constants (K_d) for SPX and GYM with *Aplysia* (A–) and *Lymnaea* (L–) AChBPs

Receptor Ligand	k_{off}, min^{-1}	k_{on}, 10^9 M^{-1} min^{-1}	K_d, nM
A–AChBP			
SPX	0.041 ± 0.023	2.2 ± 0.7	0.019
GYM	0.038 ± 0.013	8.1 ± 1.3	0.0047
L–AChBP			
SPX	0.82 ± 0.25	0.69 ± 0.07	1.2*
GYM	0.0037 ± 0.0013	2.8 ± 0.9	0.0013

Values are means ± SD from 3–6 measurements.
*A K_d of 1.26 ± 0.11 nM was alternatively determined by equilibrium titration using scintillation proximity assay for this lower affinity complex.

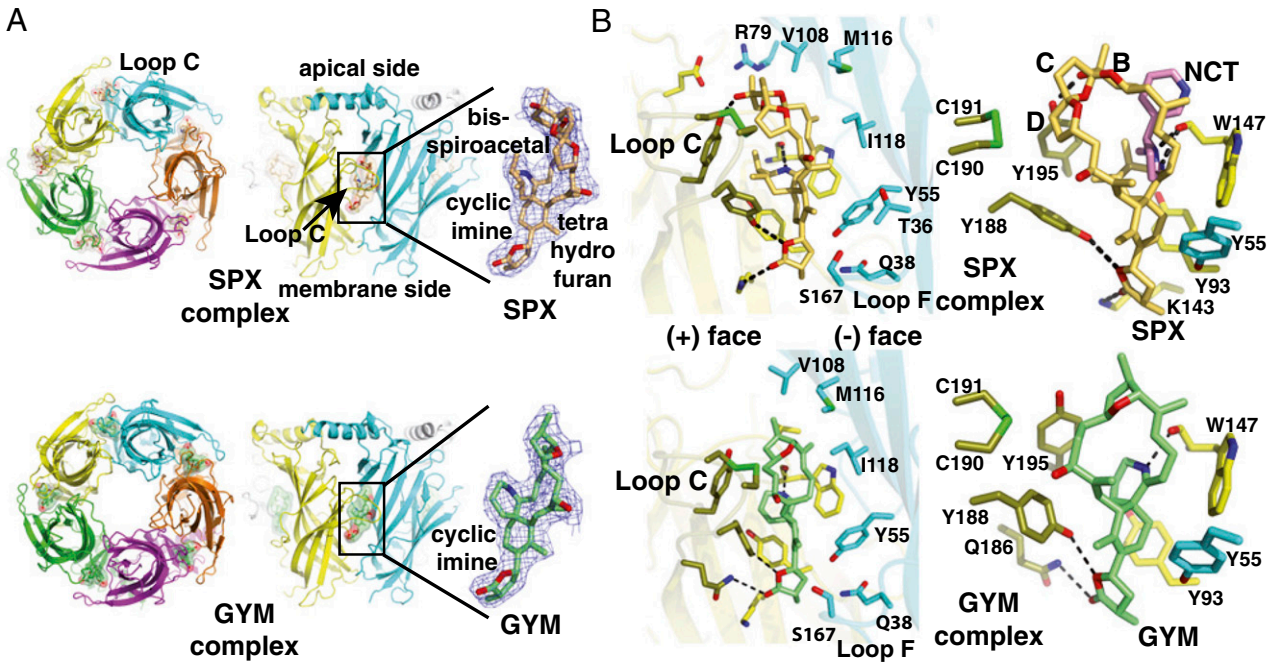

Fig. 3. Overall views of the A-AChBP pentameric complexes and subunit interfaces with bound phycotoxins. (*A*) Ribbon diagrams of the pentamer (*Left*) and subunit interface (*Center*) with bound SPX (*Upper*; orange bonds and surface, red oxygens, blue nitrogen) and GYM (Lower; green bonds and surface, red oxygens, blue nitrogen) viewed from the "membrane" side (*Left*) and radial perspectives with the apical side at top and the membrane side at bottom (*Center*). The main and side chains at the (+) and (-) faces of the interface are displayed in yellow and cyan, respectively. The bound toxins (*Right*) are perfectly ordered, as shown by their 2.5/2.4 Å resolution $2F_o$-F_c electron density maps contoured at 1.2σ (blue). (*B*) Close-up views of the bound toxins in their aromatic nest at the subunit interface, showing details of the cyclic imine environment. Bound SPX (*Upper*) is shown alone (*Left*) and overlaid with nicotine as bound to L-AChBP (pink bonds; *Right*). Bound GYM (*Lower*) is shown alone. The dashed lines denote H bonds.

carbon skeleton ideally position the cyclic imine within H bond distances (≈2.9 Å) of the carbonyl oxygen of Trp147 (loop B), as found for the pyrrolidine nitrogen in nicotine (2.6–2.7 Å) and azabicyclic nitrogen in EPI (2.7 Å). However, compared with the small pyrrolidine ring, the bulkier cyclic imine ring adopts a distinctive and nearly perpendicular orientation and stacks against Tyr93 (loop A) instead of Trp147.

The two vicinal methyl groups on the cyclic imine largely contribute to binding by abutting against the phenol rings of Tyr188 and Tyr195 from loop C (Fig. 3). The bulky and rigid *bis*-spiroacetal ring system that emerges on the apical side of the interface abuts against the tip of loop C, where it buttresses the binding interface. The preferred *cis* stereochemistry of the three-ring system, as elucidated in NMR structures of the macrocyclic toxins (28), is also observed in the AChBP complex and perfectly complements the apolar environment of the surrounding residues. In turn, the proximal tetrahydrofuran ring (ring D on Fig. 1) of the *bis*-spiroacetal ring system abuts against Tyr188, Tyr195, and the vicinal Cys190 and Cys191, whereas the central tetrahydrofuran ring (C) makes limited van der Waals contacts with Tyr195 and Cys191 from loop C and the distal tetrahydropyran ring (B) interacts with Val108 (loop E) from the (-) face. The hydroxyl and methyl substitutions on the distal tetrahydropyran ring are ideally positioned to H bond with Tyr195.

In the membrane direction of the interface, the (methyl)cyclohexene ring makes nearly edge-to-face stacking interactions with Tyr93 from the (+) face and Tyr55 (loop D) from the (-) face (Fig. 3). Its methyl group makes limited contacts with Ser167 in loop F and Thr36 in strand β1. The carbonyl and ether oxygens on the terminal (γ)-butyrolactone ring interact through weak H bonding (2.8 and 3.1 Å distances) to Lys143 and Tyr188 in AChBP.

The involvement of multiple binding loci throughout the subunit interface and the remarkable surface complementarity of the ligand and binding pocket largely explain the near pM affinity of SPX for A-AChBP (Table 3). These features also point to the cyclic imine embedded within a macrocyclic skeleton associated with the unusual *bis*-spirocetal framework as key determinants to confer the extremely potent antagonism of this class of toxins.

The Gymnodimine–AChBP Complex. The overall macrocyclic skeleton of GYM, while resembling that of SPX, also adopts a conical shape but with slightly more compact dimensions, 13 × 6 × 6 Å. The mode of binding of GYM to AChBP is very similar to that of SPX (Fig. 3) (compare rmsd values; *Materials and Methods*), with a well-conserved overall network of interactions in the two complexes (Table S3). Yet, in all five interfaces, the absence of the bulky *bis*-spiroacetal core in the GYM macrocycle is associated with a 4 Å closure movement of loop C segment Gln186-Tyr195, wrapping further around the bound GYM (Fig. 4). In turn, the solvent-exposed branch bearing the hydroxyl is displaced by 2 Å toward loop C and makes extended van der Waals contacts with Tyr195 and Cys190 in this loop, whereas the apical tetrahydrofuran ring weakly interacts with Val108 and Val148 (loop E) from the (-) face and Tyr195 from the (+) face. At the membrane side of the interface, loop C closure promotes additional interactions with the butyrolactone ring that establish weak H bonds to Lys143 and Tyr188 and van der Waals interaction with Tyr93. As in the SPX complex, very limited interactions are observed between GYM and loop F of AChBP.

The central cyclic imine of GYM virtually overlaps with that of SPX and is within H bond distance (≈2.8 Å) of the Trp147 carbonyl oxygen and virtually overlaps with that of SPX (Fig. 4). The absence of the bulky *bis*-spiroacetal ring system of SPX allows GYM to adopt a rather flat conformation within the binding pocket, a feature arguing for some conformational flexibility of the macrocyclic toxins. This comparative analysis further illustrates how loop C behaves as flexible

PHARMACOLOGY

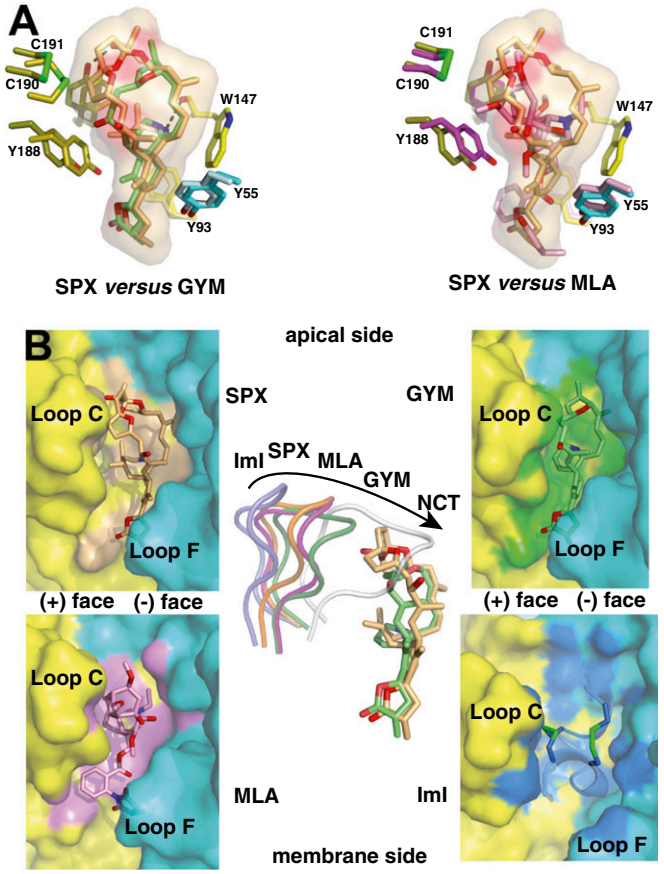

Fig. 4. Structural comparisons of the SPX and GYM complexes with other antagonist complexes. (*A*) Superimposition of SPX (orange toxin) and GYM (green) (*Left*) and SPX (orange) and MLA (pink) (*Right*) bound to A-AChBP. The molecular surface of SPX and key side chains within the binding pocket are displayed. (*B Left and Right*) Molecular surfaces buried at the A-AChBP subunit interfaces by bound SPX (orange toxin and surface), GYM (green toxin and surface), MLA (pink toxin and surface), and the peptidic α-conotoxin ImI (blue toxin with green disulfides, mauve surface), viewed radially from the pentamer outer periphery. (*B Center*) Overlay of loop C in the SPX (orange loop), GYM (green), MLA (magenta), ImI (blue) and nicotine (white) complexes as viewed from the pentamer apical side, also showing overlaid bound SPX and GYM molecules.

sensor to adapt its configuration to the chemical features of the ligand entering the binding pocket, as previously documented for several structurally unrelated nicotinic ligands (Fig. 4) (21, 24, 25).

Unique Structural Features of SPX and GYM. Overall, the mode of binding of SPX and GYM to A-AChBP, when compared with muscle and neuronal nAChRs (Table S3 and Fig. S1), defines the determinants for high affinity and limited selectivity in nAChRs. In fact, both the SPX and GYM complexes show little involvement of the sequence-variable loop F in ligand binding. The macrocyclic structure of these toxins ensures an ideal positioning of the central cyclic imine as a hinge point. Most importantly, the architectural constraints of the unusual macrocyclic ring structures stabilize conformers with strategically positioned substituents that confer high surface complementarity and minimize the loss of entropy as toxins bind to A-AChBP (Fig. 4). Indeed, SPX and GYM are deeply anchored/buried at the binding interface, resulting in surface areas of ≈550 Å^2 (out of 835 Å^2 for the entire toxin molecule) and ≈430 Å^2 (out of 705 Å^2) buried to a 1.4 Å probe radius, respectively. The role of particular substituents in selectivity of several SPX and GYM congeners is discussed in the *SI Appendix*.

Comparison with Other Nicotinic Antagonists. Certain features of the A-AChBP complexes with SPX and GYM closely resemble the complex with the antagonist, methyllycaconitine (MLA) (compare rmsd value; *Materials and Methods*), in particular the position/conformation of loop C (Fig. 4). In fact, the bulky oxygen-rich lycaconitine skeleton of MLA behaves similarly to the carbon skeleton of SPX, in preventing loop C to adopt a tightly closed conformation (Fig. 4). Structure overlay shows that Tyr188 is capable of adopting distinct positions to optimize interactions with the bound ligand. In contrast however, the *bis*-spiroacetal ring system of SPX apical to the interface has no equivalent in MLA, a feature arguing for a chemically important moiety to confer the high potency of SPX and related toxins. This feature obviously accounts for the up to 600-fold higher affinity of the phycotoxins for the AChBPs compared to MLA (K_d values of 2.8 nM and 0.41 nM for A- and L-AChBP, respectively; ref. 24). The loop C conformation in the SPX and GYM complexes also resembles that observed in apo A-AChBP and termed "intermediate," as compared with the "open" and "closed" conformations, respectively, associated with binding of the peptidic antagonist, α-conotoxin ImI, and the small organic agonists, EPI and lobeline (compare rmsd value; *Materials and Methods*).

The peptidic α-conotoxin ImI covers the apical and central surfaces of the binding pocket and extends toward loop F, features accounting for its selectivity toward neuronal nAChRs (Fig. 4). Structural comparison with other nicotinic antagonists bound to AChBP (24) reveals that this unique class of macrolide polyether toxins exploit extended and nonoverlapping interaction surface regions at both the apical and membrane sides of the subunit interface for stabilization of their complexes. This comparison also suggests substituent modification at key positions around the macrocyclic framework of dinoflagellate toxins to confer binding selectivity and specificity.

Concluding Remarks. The unique spiroimine structures can be related to those of other small alkaloid molecules to further define the specificity of marine versus terrestrial toxins. Compared with another alkaloid, terpine, and to the peptidic toxins, a unique feature of the large spiroimine macrocylic structure is its extension in both the membrane and apical directions of the AChBP ring along the subunit interface, encompassing all or large part of the binding surface of other antagonists. A second feature is the presence of a cyclic, six- or seven-membered imine ring structure also found in the anabaseines (29). The spectroscopic characteristics of the benzylidene anabaseines enabled one to establish that the imine nitrogen is protonated in the bound state through measuring difference spectra of the bound and free ligands (30). The cembranoids from coral are also macrocyclic inhibitors containing internal lactones, but they lack a protonatable nitrogen. Although the cembranoids alter nicotinic receptor function, there is no evidence for competitive interactions at the agonist site (31). The lophotoxins from coral have a similar macrocyclic terpenoid structure, devoid of a nitrogen (32), but they react covalently through an epoxide moiety with the nicotinic receptor producing a slow progressive inhibition (33).

Hence, the marine toxins display a great diversity of means of interaction with nicotinic receptors. In the case of the competitive dinoflagellate toxins considered here, the macrocyclic entities lack the reactive moieties to form stable covalent bonds. Rather, the precise positioning of the ligand through imine H bond donation, coupled with the exquisite complementarity of the macrocycle outside shell with the side chains at the subunit interface, gives rise to the high affinity and slow dissociation of the bound ligand that account for apparent irreversibility over a short time frame. These data offer a unique template for the design of novel drugs with high affinity and limited receptor subtype selectivity. Moreover, AChBP-based binding assays may prove more sensitive and versatile than the official broad spectrum mouse bioassay reference (http://www.efsa.europa.eu) for spiroimine toxin detection in contaminated waters and seafood.

Materials and Methods

Live Animals and Biological Materials. Their sources are stated in the *SI Appendix*.

nAChR Preparation and Expression and Binding Assays. *Torpedo marmorata* membranes enriched in $\alpha 1_2\beta\gamma\delta$ nAChR (34) were resuspended in 5 mM glycine and stored at −80 °C. Equilibrium competition on $\alpha 1_2\beta\gamma\delta$ used 0.05 μg of membranes (≈100 pM in toxin binding sites), 0.25–0.35 nM ^{125}I-BgTx (L*) and a range of SPX and GYM concentrations (≥ 4-h incubation, 20–25 °C) (35). Unbound and bound ^{125}I-BgTx were separated by filtration. cDNAs encoding human α3β2 and α4β2 nAChRs were transfected into HEK-293 cells (35). Equilibrium competition on α3β2 and α4β2 used a cell density adjusted to specifically bind ≤10% of radioligand, 0.5 nM [^{3}H]-EPI (L*) and a range of SPX and GYM concentrations (4-h incubation, 20–25 °C) (15). Unbound and bound [^{3}H]-EPI were separated by filtration. IC_{50} values were determined as described in *SI Appendix*.

nAChR Microtransplantation and Expression in Oocytes, and Voltage-Clamp recording. Stage V-VI *Xenopus* oocytes free of follicular cells were maintained in Barth's solution supplemented with antibiotics (15). Transplantation of *Torpedo* $\alpha 1_2\beta\gamma\delta$ nAChR used microinjection, into the oocyte cytoplasm, of a membrane suspension (50 nL at 3.5 mg/mL protein) from a Nanoliter2000 Micro4 Controller mounted on a microscope (36). Expression of human α4β2 nAChR used microinjection, into the oocyte nucleus, of a 1:1 mixture of cDNA (50 nL at 0.28 μg/μl) encoding α4 and β2 subunits in a pRc/CMV expression vector and a Nanoliter2000 microinjector (15). Oocytes were maintained at 18 °C and voltage-clamp recordings performed 3–5 days later. ACh-evoked currents were recorded with a standard two-microelectrode voltage-clamp technique at a holding potential of −60 mV (15), and dose-response curves for agonist activation were analyzed and IC_{50} values determined, as described in *SI Appendix*.

Ligand Binding to AChBP. A- and L-AChBP were expressed and purified according to refs. 22 and 24, and rate constants for association (k_{on}) and dissociation (k_{off}) were determined by multiple kinetic means to cover the wide range of values observed (Table 3) as described in *SI Appendix*.

Crystallization, Data Collection, Structure Determination and Refinement. A-AChBP complexes were formed and crystallized and data were processed as described in *SI Appendix*. The structures of the SPX- and GYM-A-AChBP complexes were solved by molecular replacement with MOLREP using the apo A-AChBP structure (PDB code 2BYN) (24) as a search model. Details of the refinement procedure and structural comparisons are described in *SI Appendix*. The final structures comprise residues His1-Arg208 for each of the five subunits in the pentamer and a fully resolved ligand molecule in each of the five binding sites within the pentamer. Virtually all of the N-terminal FLAG sequence is clearly visible in most subunits, but high temperature factors and weak electron density are associated with surface loops Asn15-Met19 and Asp68-Gln71. Fig. 1 was generated with ChemDraw (CambrigeSoft) and Figs. 3 and 4 with PyMOL (37).

ACKNOWLEDGMENTS. We gratefully acknowledge the expert assistance of Kwok-Yiu Ho for AChBP binding assays, Amélie Goudet for nAChR binding experiments, Sandrine Conrod for crystallization, and Gerlind Sulzenbacher and the ID14 and ID23 staff of the European Synchrotron Radiation Facility for data collection. We thank Jean-Pierre Changeux and Ortrud Steinlein for providing cDNAs. This work was supported by Agence Nationale de la Recherche Grant PCV07-194417-Neurospiroimine and STC-CP2008-1-555612 (ATLANTOX) Grant (to J.M.), US Public Health Service Grants R37-GM18360 and P42-ES-010337 (to P.T.), and a Centre National de la Recherche Scientifique-Office of International Relations travel grant (to P.M.).

1. Ciminiello P, Fattorusso E (2006) Bivalve molluscs as vectors of marine biotoxins involved in seafood poisoning. *Prog Mol Subcell Biol* 43:53–82.
2. Gill S, et al. (2003) Neural injury biomarkers of novel shellfish toxins, spirolides: A pilot study using immunochemical and transcriptional analysis. *Neurotoxicology* 24:593–604.
3. O'Connor PD, Brimble MA (2007) Synthesis of macrocyclic shellfish toxins containing spiroimine moieties. *Nat Prod Rep* 24:869–885.
4. Cembella AD, Lewis NI, Quilliam MA (1999) Spirolide composition of micro-extracted pooled cells isolated from natural plankton assemblages and from cultures of the dinoflagellate Alexandrium ostenfeldii. *Nat Toxins* 7:197–206.
5. Hu T, et al. (2001) Characterization of spirolides a, c, and 13-desmethyl c, new marine toxins isolated from toxic plankton and contaminated shellfish. *J Nat Prod* 64:308–312.
6. Aasen J, et al. (2005) Detection and identification of spirolides in norwegian shellfish and plankton. *Chem Res Toxicol* 18:509–515.
7. Cembella AD, Lewis NI, Quilliam MA (2000) The marine dinoflagellate Alexandrium ostenfeldii (Dinophyceae) as the causative organism of spirolide shellfish toxins. *Phycologia* 39:67–74.
8. MacKinnon SL, et al. (2006) Spirolides isolated from Danish strains of the toxigenic dinoflagellate Alexandrium ostenfeldii. *J Nat Prod* 69:983–987.
9. Ciminiello P, et al. (2007) Spirolide toxin profile of Adriatic Alexandrium ostenfeldii cultures and structure elucidation of 27-hydroxy-13,19-didesmethyl spirolide C. *J Nat Prod* 70:1878–1883.
10. Molgó J, Girard E, Benoit E (2007) The cyclic imines: An insight into this emerging group of bioactive marine toxins. *Phycotoxins: Chemistry and Biochemistry*, ed Botana LM (Blackwell Publishing Ltd., Iowa), pp 319–335.
11. Richard D, Arsenault E, Cembella A, Quilliam MA (2001) Investigations into the toxicology and pharmacology of spirolides, a novel group of shellfish toxins. *Harmful Algal Blooms 2000*, eds Hallegraeff GM, Blackburn SI, Bolch CJ, Lewis RJ (Intergovernmental Oceanographic Commission of UNESCO, Paris), pp 383–386.
12. Seki T, Satake M, Mackenzie L, Kaspar HF, Yasumoto T (1995) Gymnodimine, a new marine toxin of unprecedented structure isolated from New Zealand oysters and the dinoflagellate Gymnodinium sp. *Tetrahedron Lett* 36:7093–7096.
13. Miles CO, Wilkins AL, Stirling DJ, MacKenzie AL (2000) New analogue of gymnodimine from a Gymnodinium species. *J Agric Food Chem* 48:1373–1376.
14. Miles CO, Wilkins AL, Stirling DJ, MacKenzie AL (2003) Gymnodimine C, an isomer of gymnodimine B, from Karenia selliformis. *J Agric Food Chem* 51:4838–4840.
15. Kharrat R, et al. (2008) The marine phycotoxin gymnodimine targets muscular and neuronal nicotinic acetylcholine receptor subtypes with high affinity. *J Neurochem* 107:952–963.
16. Munday R, et al. (2004) Acute toxicity of gymnodimine to mice. *Toxicon* 44:173–178.
17. Changeux JP, Edelstein SJ (2005) Allosteric mechanisms of signal transduction. *Science* 308:1424–1428.
18. Taylor P (2006) Agents acting at the neuromuscular junction and autonomic ganglia. *Goodman and Gilman's The Pharmacological Basis of Therapeutics*, eds Brunton LL, Lazo JS, Parker KL (McGraw–Hill, New York), pp 217–236.
19. Le Novère N, Corringer PJ, Changeux JP (2002) The diversity of subunit composition in nAChRs: Evolutionary origins, physiologic and pharmacologic consequences. *J Neurobiol* 53:447–456.
20. Brejc K, et al. (2001) Crystal structure of an ACh-binding protein reveals the ligand-binding domain of nicotinic receptors. *Nature* 411:269–276.
21. Celie PH, et al. (2004) Nicotine and carbamylcholine binding to nicotinic acetylcholine receptors as studied in AChBP crystal structures. *Neuron* 41:907–914.
22. Hansen SB, et al. (2002) Tryptophan fluorescence reveals conformational changes in the acetylcholine binding protein. *J Biol Chem* 277:41299–41302.
23. Bourne Y, Talley TT, Hansen SB, Taylor P, Marchot P (2005) Crystal structure of a Cbtx-AChBP complex reveals essential interactions between snake α-neurotoxins and nicotinic receptors. *EMBO J* 24:1512–1522.
24. Hansen SB, et al. (2005) Structures of Aplysia AChBP complexes with nicotinic agonists and antagonists reveal distinctive binding interfaces and conformations. *EMBO J* 24:3635–3646.
25. Hibbs RE, et al. (2009) Structural determinants for interaction of partial agonists with acetylcholine binding protein and neuronal alpha7 nicotinic acetylcholine receptor. *EMBO J* 28:3040–3051.
26. Sine SM, Taylor P (1981) Relationship between reversible antagonist occupancy and the functional capacity of the acetylcholine receptor. *J Biol Chem* 256:6692–6699.
27. Hansen SB, Talley TT, Radić Z, Taylor P (2004) Structural and ligand recognition characteristics of an acetylcholine-binding protein from Aplysia californica. *J Biol Chem* 279:24197–24202.
28. Falk M, Burton IW, Hu T, Walter JA, Wright JLC (2001) Assignment of the relative stereochemistry of the spirolides, macrocyclic toxins isolated from shellfish and from the cultured dinoflagellate Alexandrium ostenfeldii. *Tetrahedron* 57:8659–8665.
29. Kem W, et al. (2006) The nemertine toxin anabaseine and its derivative DMXBA (GTS-21): Chemical and pharmacological properties. *Mar Drugs* 4:255–273.
30. Talley TT, et al. (2006) Spectroscopic analysis of benzylidene anabaseine complexes with acetylcholine binding proteins as models for ligand-nicotinic receptor interactions. *Biochemistry* 45:8894–8902.
31. Hann RM, et al. (1998) Characterization of cembranoid interaction with the nicotinic acetylcholine receptor. *J Pharmacol Exp Ther* 287:253–260.
32. Abramson SN, et al. (1991) Structure/activity and molecular modeling studies of the lophotoxin family of irreversible nicotinic receptor antagonists. *J Med Chem* 34:1798–1804.
33. Groebe DR, Abramson SN (1995) Lophotoxin is a slow binding irreversible inhibitor of nicotinic acetylcholine receptors. *J Biol Chem* 270:281–286.
34. Hill JA, Jr, Nghiêm HO, Changeux JP (1991) Serine-specific phosphorylation of nicotinic receptor associated 43K protein. *Biochemistry* 30:5579–5585.
35. Servent D, et al. (1997) Only snake curaremimetic toxins with a fifth disulfide bond have high affinity for the neuronal α7 nicotinic receptor. *J Biol Chem* 272:24279–24286.
36. Krieger F, et al. (2008) Fluorescent agonists for the Torpedo nicotinic acetylcholine receptor. *ChemBioChem* 9:1146–1153.
37. Delano WL (2002) *The PyMOL* molecular graphics system (DeLano Scientific LLC, Palo Alto, CA).